ACS Biomaterials SCIENCE & ENGINEERING

pubs.acs.org/journal/abseba

Article

Long-Term in Vivo Performance of Low-Temperature 3D-Printed Bioceramics in an Equine Model

Rafael Vindas Bolaños,[#] Miguel Castilho,[*,#] Janny de Grauw, Stefan Cokelaere, Saskia Plomp, Jürgen Groll, P. René van Weeren, Uwe Gbureck, and Jos Malda

Cite This: *ACS Biomater. Sci. Eng.* 2020, 6, 1681−1689

Read Online

ACCESS | Metrics & More | Article Recommendations

ABSTRACT: Bone has great self-healing capacity, but above a certain critical size, bone defects will not heal spontaneously, requiring intervention to achieve full healing. Among the synthetic calcium phosphate (CaP) bone replacement materials, brushite ($CaHPO_4{\cdot}2H_2O$)-based materials are of particular interest because of their degree of solubility and the related high potential to promote bone regeneration after dissolution. They can be produced tailor-made using modern three-dimensional (3D) printing technology. Although this type of implant has been widely tested in vitro, there are only limited in vivo data and less so in a relevant large animal model. In this study, material properties of a 3D-printed brushite-based scaffold are characterized, after which the material is tested by in vivo orthotopic implantation in the equine tuber coxae for 6 months. The implantation procedure was easy to perform and was well tolerated by the animals, which showed no detectable signs of discomfort. In vitro tests showed that compressive strength along the vertical axis of densely printed material was around 13 MPa, which was reduced to approximately 8 MPa in the cylindrical porous implant. In vivo, approximately 40% of the visible volume of the implants was degraded after 6 months and replaced by bone, showing the capacity to stimulate new bone formation. Histologically, ample bone ingrowth was observed. In contrast, empty defects were filled with fibrous tissue only, confirming the material's osteoconductive capacity. It is concluded that this study provides proof that the 3D-printed brushite implants were able to promote new bone growth after 6 months' implantation in a large animal model and that the new equine tuber coxae bone model that was used is a promising tool for bone regeneration studies.

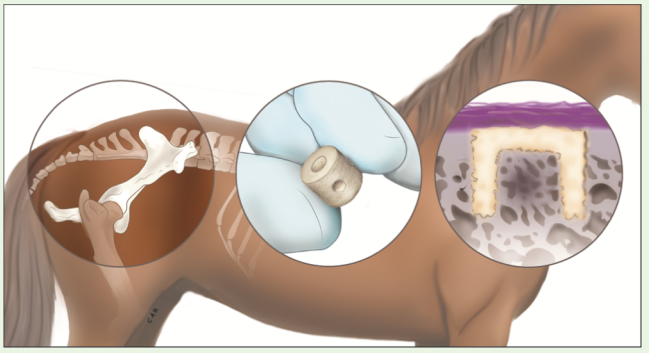

KEYWORDS: *calcium phosphates, three-dimensional printing, in vivo, equine model, osteoconduction, osteoinduction*

1. INTRODUCTION

Bone is a complex dynamic tissue that provides biomechanical stability to the body and plays an important role in hematopoietic cell production and calcium homeostasis.[1] Despite the self-healing capabilities of bone, bone defects with geometries larger than their critical healing size (≈10 mm) do not stand a chance to heal at all. In such situations, there is a need for external intervention to support bone repair, for example, by grafting with biomaterials or harvested bone.[2] After decades of intensive bone research, autografting procedures remain the gold standard in orthopedic surgery. Bone autografts can guide the ingrowth of osteoblasts and induce the differentiation of undifferentiated bone cells into the osteogenic lineage.[3] Unfortunately, autografting is associated with donor site morbidity and limited availability. As an alternative, a broad spectrum of bone graft biomaterials has been investigated.[4,5]

Among the different types of candidate biomaterials, synthetic ceramics, usually based on calcium phosphate (CaP) chemistry, are of particular interest due to their similar composition to bone mineral and resorption potential. There are several known CaPs, with CaP phases depending on their calcium-to-phosphate (Ca/P) molar ratio.[6] The most common are hydroxyapatite (HA), tricalcium phosphate (TCP) in two crystalline forms, β-tricalcium phosphate (β-TCP) and α-tricalcium phosphate (α-TCP), and dicalcium phosphate dihydrate (or brushite). The performance of these CaPs is greatly dependent upon specific material properties. It is known that phase composition, crystal size, and porosity are the key factors that determine the speed of resorption and mechanical stability of these materials, as well as their subsequent success or failure in promoting bone regeneration

Received: November 30, 2019
Accepted: January 31, 2020
Published: January 31, 2020

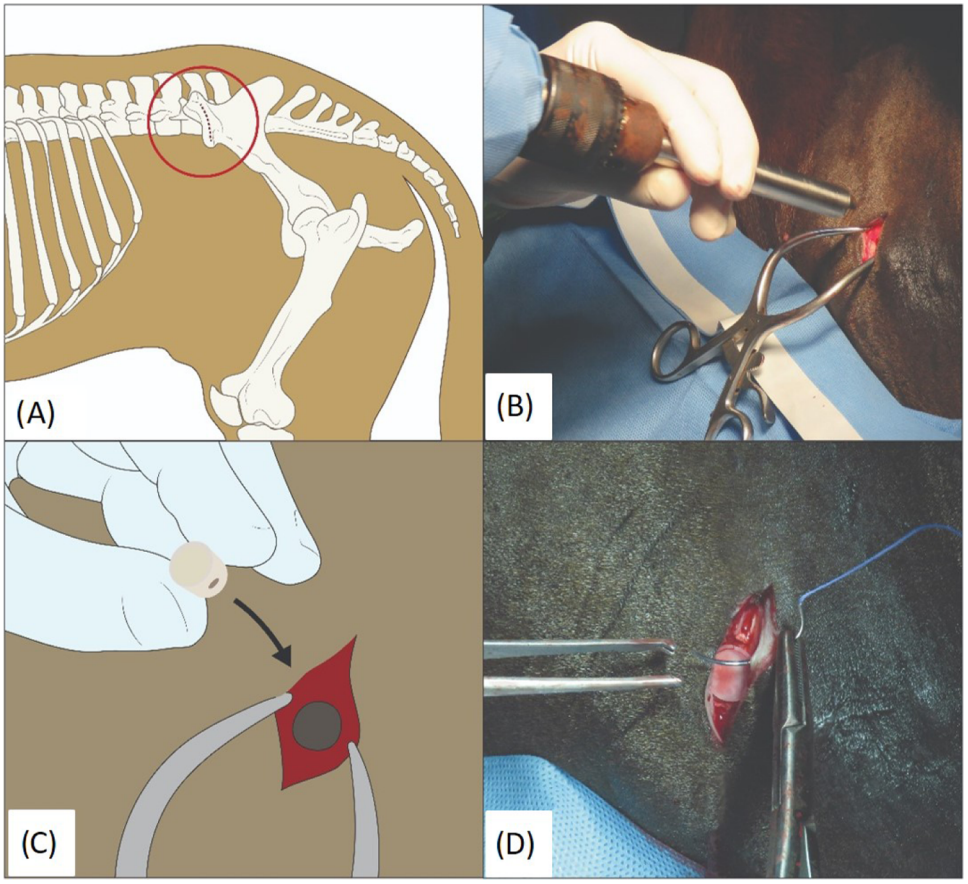

Figure 1. Surgical implantation of 3D-printed ceramic implants in the tuber coxae model. (A) Position of the tuber coxae of the ileum wing in the horse. (B) The defect was made using a power drill. (C) Schematic drawing of placement of the scaffold into the defect. (D) Wound closure.

in vivo.[7] While sintered hydroxyapatite is practically non-degradable in vivo, TCP or brushite are more soluble phases with higher potential to promote bone regeneration after dissolution.[8,9] These unique characteristics have drawn increasing attention to brushite-based materials.[10,11]

In case of large and complex bone defects, the capacity to mold the biomaterial according to the shape needed, together with the desired rate of biodegradation, is a determining factor. Such bone defects can hardly be treated with pasty bone materials, but require the implantation of preformed bone scaffolds, often with complex geometry.[12,13] Current CaP bone substitutes are mostly available as injectable pastes or in standard shapes that do not fit patient-specific defect requirements. Recently, we have shown that three-dimensional powder printing (3DPP) is a promising manufacturing technique for the fabrication of individual ceramic-based bone grafts.[14−16] In previous works, we have used a low-temperature processing regime to produce personalized ceramic matrices composed of TCP and/or brushite mineral phases.[14,15] The suitability of these materials for bone replacement has been confirmed by few in vivo implantation experiments. Habibovic et al. tested 3D-printed brushite-based scaffolds on the decorticated lumbar transverse processes of goats for 3 months,[10] while Tamimi et al. tested implants with a similar composition in a calvarial bone surface of rabbits.[17] Although promising, translational animal studies of biomaterial performance for intended human application should ideally be performed in large animal species, as small laboratory animals possess superior regenerative ability compared to humans and larger animals.[18] Also, in vivo studies should be of sufficient duration to allow assessment of long-term effects and durability.[19]

In fact, there is still no consensus on the ideal in vivo model to study the osteopromotive potential of biomaterials. In orthopedic regenerative medicine, however, evaluation of novel interventions in large animal models is a prerequisite to human clinical application, while such studies constitute end-stage testing for veterinary application in the animal species involved.[20] Similar to humans and unlike other perhaps more common animal model species like goats or sheep, horses participate in athletic competitions, where osteochondral injuries cause great economic losses as well as raise animal welfare concerns.[21−23] Studies addressing bone regenerative capacity are, therefore, also of potential interest for equine health care and welfare.

The aim of this study was to characterize the material properties of 3D-printed brushite-based scaffolds as well as to evaluate their in vivo orthotopic bone regenerative potential in a long-term equine animal study. The structural and mechanical properties of the printed materials were carefully investigated prior to implantation. For the in vivo evaluation, experimentally created defects in the equine tuber coxae bone were used as a new model for large animal preclinical bone regeneration studies. Implants with a cylindrical geometry and an interconnected macroporosity were used with the intention that they might serve as potential osteal anchors of hydrogel-based chondral implants in future studies. Implants were inserted into experimentally created defects in the tuber coxae

https://dx.doi.org/10.1021/acsbiomaterials.9b01819
ACS Biomater. Sci. Eng. 2020, 6, 1681−1689

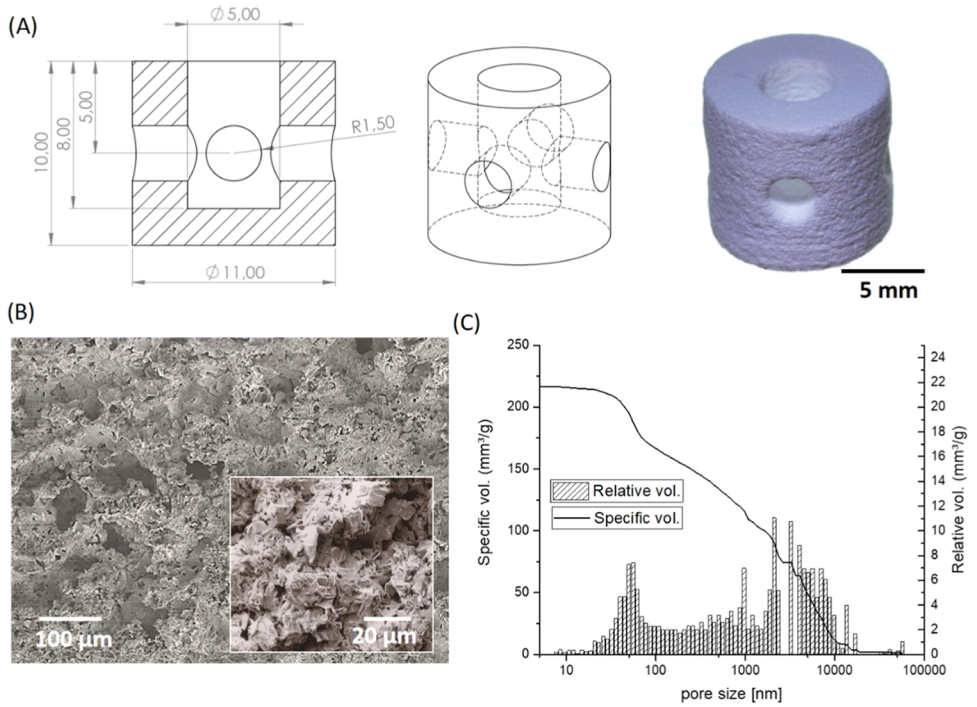

Figure 2. Implant design and structural characterization. (A) CAD design and photograph of the printed implant. (B) Implant microstructure and (C) pore size distribution prior to implantation.

of n = 8 horses and were retrieved 6 months after implantation; implant degradation and bone regeneration were evaluated by micro-computed tomography (μCT) and histological analyses.

2. MATERIALS AND METHODS

2.1. Implant Preparation and Material Characterization. Ceramic implants (cylindrical diameter = 11 mm, depth = 10 mm with open channel diameter 3 mm, Figure 1) and dense samples for structural and mechanical testing were printed from α/β-TCP (α/β-Ca_3PO_4) powder and 20% v/v phosphoric acid binder (Merck, Darmstadt, Germany) on a Z-Corp 310 (Z-Corporation, Burlington) powder printer. A detailed description of powder synthesis and printing process parameters is provided elsewhere.[14] After removal from the powder bed, the printed constructs were cleaned with compressed air and posthardened by immersion in the binding liquid for 2 × 30 s to increase the degree of cement setting. Microporosity and pore size distribution characteristics of the 3D-printed constructs were measured with Hg porosimetry (PASCAL 140/440, Porotec GmbH, Hofheim, Germany). The microstructure was visualized using scanning electron microscopy (SEM) Phenom Pro (Phenom-World, The Netherlands), at an acceleration voltage of 5−10 kV. Prior to scanning, specimens were sputter-coated with a 5 nm layer of gold.

2.2. Mechanical Characterization. Mechanical properties were evaluated under two stress-loading conditions by performing uniaxial compression and diametral compression tests. Dense specimens of appropriate geometry and printed according to the three directions of the printing process, x, y, and z, were used. All tests were performed with a universal testing machine, Zwick/Roell Z010 (Zwick GmbH & Co. KG, Ulm, Germany), equipped with a 5 kN load cell, according to a protocol described elsewhere.[24] Briefly, for uniaxial compression, dense cylindrical samples with height = 12 mm and diameter = 6 mm were tested at a rate of 1 mm/min. Compressive strength (CS) was defined as the ratio between the force at failure and the specimen's unloaded cross-sectional area. For diametral compression, disk-shaped specimens with a thickness = 4 mm and diameter = 8 mm were tested at 0.5 mm/min. The diametral tensile strength (DTS) was calculated by

$$\mathrm{DTS\ (MPa)} = 2F_{max}/(\pi dt) \quad (1)$$

where F_{max} is the failure load and d and t are the sample diameter and thickness, respectively. Implant compressive strength was only determined under axial compression and calculated on the basis of cross-sectional area of the bottom of the implant without considering the central or horizontal pores.

2.3. Experimental Design. The protocols and study described were approved by the ethical and animal welfare committee of the National University of Costa Rica Veterinary School. Eight healthy Criollo breed horses (five mares, three geldings; mean age, 6 years, range, 4−9 years; mean body weight, 288 kg, range, 275−350 kg) were used. All horses were free of lameness and did not have clinical or radiographic evidence of acute or chronic injuries. They were housed in individual box stalls and were fed a standard maintenance ration of 0.5 kg concentrate daily, with hay ad libitum and free access to water.

2.4. Surgical Procedure. After IV premedication with xylazine (1.1 mg/kg; Pisa, Mexico), a 12G jugular venous catheter was placed and phenylbutazone (2.2 mg/kg; Holliday, Argentina) administered IV for perioperative analgesia. Anesthesia was induced with midazolam (0.05 mg/kg; Holliday, Argentina) IV and ketamine (2.2 mg/kg; Holliday, Argentina) IV, and the horse was positioned in dorsal recumbence. General anesthesia was maintained with isoflurane in oxygen.

For the tuber coxae model, a vertical incision through the skin and subcutaneous tissue of approximately 10 cm length was made by a board-certified equine surgeon (SC) over the tuber coxae to expose the underlying bone (Figure 2). Once the bony surface of the tuber coxae was exposed, one cylindrical defect (11 mm diameter, 10 mm depth) was created perpendicular to the bony surface using a stop-controlled power-driven drill. Defects were flushed with saline (Baxter) before press-fit implantation of the scaffolds (n = 8). Control defects (n = 8) of the same size and depth were created in a similar fashion in the contralateral tuber coxae and were left empty. Finally, the skin was closed using nylon sutures (Ethilon 0). These surgeries were performed during the same anesthetic episode as was used for the surgical creation of osteoarticular defects in both stifle joints for an unrelated cartilage repair study that has been reported elsewhere.[25]

https://dx.doi.org/10.1021/acsbiomaterials.9b01819
ACS Biomater. Sci. Eng. 2020, 6, 1681−1689

2.5. Postoperative Care and Rehabilitation. Postoperatively, the horses received antibiotics for 8 days (procaine penicillin 15 000 IU/kg intramuscularly SID, Alfasan, and IV gentamicin 6.6 mg/kg BID, Alfasan) and nonsteroidal anti-inflammatory drugs (phenylbutazone [2.2 mg/kg, Lisan, orally BID]) during the first 14 days. As the horses were enrolled in a parallel cartilage repair study, from week 3, they were subjected to an incremental exercise program as detailed elsewhere.[25]

2.6. Monitoring during Experimental Period. The animals were clinically monitored on a daily basis for rectal temperature, heart rate, and respiratory rate, as well as stance, demeanor, and general appearance; hematology and serum biochemistry were checked 1, 2, 4, and 6 months, postoperatively.

2.7. Euthanasia and Sample Harvesting. All horses were euthanized at 6 months postoperatively using a combination of xylazine (1 mg/kg IV, Pisa) and ketamine-midazolam (3 mg/kg and 0.05 mg/kg IV, Holliday) to induce profound anesthesia. After this, a bolus of oversaturated magnesium sulfate (200 g/L) and chloral hydrate (200 g/L) solution was administered to effect, and death was confirmed by cessation of breathing, ictus, and corneal reflex.

After opening the skin and subcutaneous tissue over the tuber coxae, macroscopic pictures were taken and blocks of tissue containing the defects were excised. A piece containing the treated defect was fixed in 10% formalin for micro-CT analysis, X-ray diffraction analysis, and histological evaluation after embedding in poly(methylmethacrylate) (MMA).

2.8. Micro-Computed Tomography and X-ray Diffraction. To visualize the calcified tissue at the defect site, the formalin-fixed tissue underwent micro-CT analysis (Quantum FX-PerkinElmer). The newly fabricated implants were also analyzed with micro-CT. The scan parameters were 90 kV tube voltage, 180 mA tube current, 60 μm resolution, and 3 min scan time. Reconstruction of two-dimensional projections was automatically performed using the inbuilt software of the micro-CT, while preprocessing (image calibration and noise reduction) of the images was undertaken with Analyze-11.0 software. Implant degradation was quantified by comparing the reconstructed volumes of the implants before and after 6 months of implantation. Before and 6 months after the implantation, the diffraction patterns of the ceramic implants were analyzed using a powder diffractometer (D5005, Siemens, Karlsruhe, Germany) with monochromatic Cu K_1 radiation at an acceleration voltage of 40 kV. Data were collected in a 2θ range of 20−40° with a step size of 0.02°. Diffraction patterns were qualitatively analyzed using the following reference patterns from the powder diffraction database: brushite (PDF-ref 09-0077), monetite (PDF-No. 09-0080), α-TCP (PDF-ref 09-0348), β-tricalcium phosphate (PDF-ref 09-0169), and hydroxyapatite (HA) (PDF-ref 09-0432).

2.9. Histological Processing. The tuber coxae bone samples were fixed in neutral buffered formalin at 10% and dehydrated through an ethanol series, cleared in xylene and embedded in MMA. Embedded samples were cut with a Leica 4 SP1600 Saw Microtome system (Leica, Germany) to yield 20−30 μm sections. The sections were stained with methylene blue and basic fuchsin for analysis of tissue−scaffold integration and bone growth. The samples were also stained with picrosirius red and analyzed with polarized light for collagen analysis. Stained sections were imaged using an Olympus BX51 light microscope.

2.10. Statistical Analysis. A one-way ANOVA post hoc test (Tukey's test) was used to compare the means of the different groups. Differences were considered significant at a probability error (p) of <0.05.

3. RESULTS

3.1. 3D-Printed Material Characterization. Implants were successfully 3D-printed based on the hydraulic setting reaction of a reactive α/β-TCP powder with a phosphoric acid binder. This reaction led to the precipitation of brushite and, thus, to the formation of a stable 3D structure (Figure 1A). No significant dimensional changes were observed between the as-printed constructs and the computer-designed geometry. Evaluation of the implants' dimensions revealed a deviation of less than ±0.1 mm.

While analyzing the printed constructs' microstructure, we observed that all specimens had a porous microstructure composed of randomly oriented brushite crystals (Figure 1B). The total microporosity of all specimens was in the range of 28−30 vol %, with a bimodal pore size distribution and with the main pore size fraction in the range of 90 nm to 10 μm (Figure 1C).

The results from compression strength testing revealed no significant differences between the three different directions, with final strengths of approximately 13 MPa (Figure 3). In contrast, the tensile strength was significantly higher for the samples printed along the z direction compared to the x and y directions, with strengths reaching approximately 2.2 MPa (Figure 3). As expected for a ceramic material, printed constructs were stronger under compression and weaker under tensile load. Based on both compression and tensile strength, macroporous implants for subsequent in vivo tests were printed along the z direction and tested under compressive loading. The stress−strain behavior of macroporous implants was similar to that of the dense specimens. However, a significant decrease in compression strength, from approximately 13 to 8.2 ± 2.1 MPa, was observed.

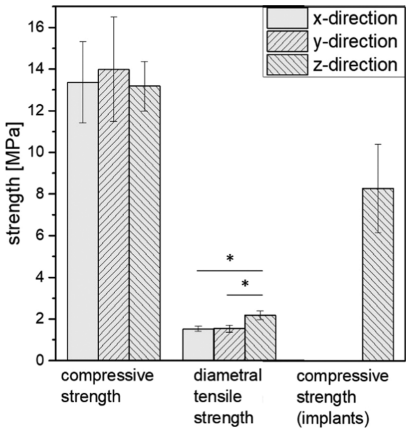

Figure 3. Mechanical properties of densely printed brushite material. Compressive strength (CS) and diametral tensile strength (DTS) were evaluated in three different directions of the printing process. Of the porous implants, uniaxial compressive strength only was determined prior to implantation.

3.2. Surgery, Postoperative Care, and Monitoring. The surgical procedure proved straightforward, with the approach providing ample access to the proposed defect site (Figure 2). Defect creation was likewise easily performed, as was press-fit implantation of scaffolds. Postoperatively, seven out of eight horses recovered uneventfully and had uncomplicated healing of the surgical incisions. One horse showed signs of a local surgical site infection (tenderness, swelling, drainage) 3 days after surgery, which was treated with antibiotics and cleaning; signs resolved within the first week postoperatively. In all other horses, no local tissue reaction or signs of infection (heat, pain, swelling) were seen. In all horses, routine blood parameters remained within normal physiologic limits throughout the experiment.

3.3. Micro-CT and Phase Composition Analysis. Micro-CT analysis was performed on the tuber coxae

https://dx.doi.org/10.1021/acsbiomaterials.9b01819
ACS Biomater. Sci. Eng. 2020, 6, 1681−1689

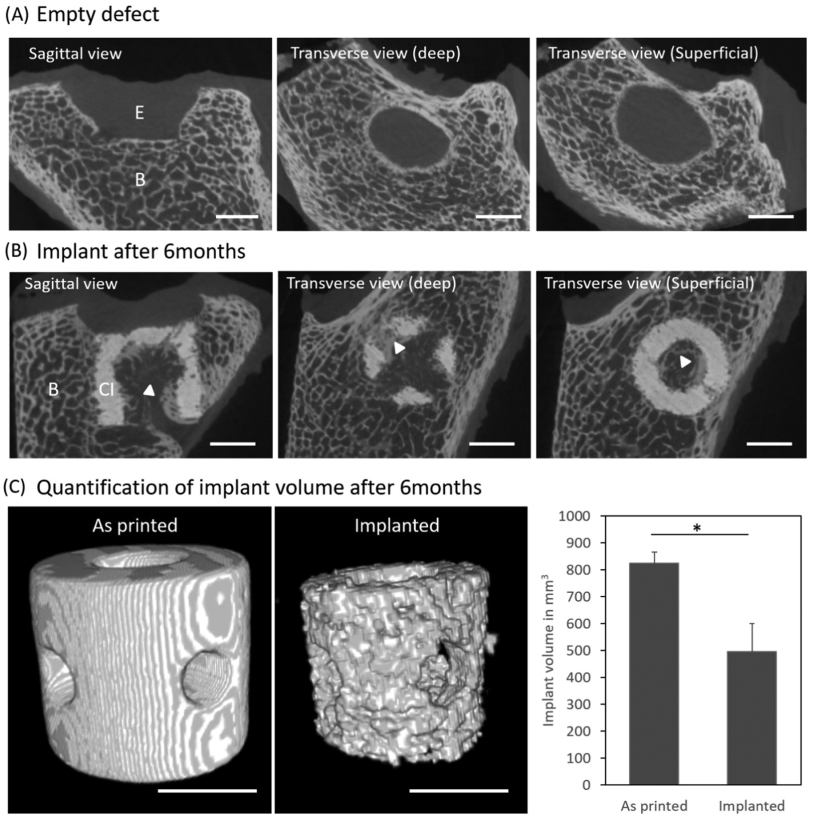

Figure 4. μCT analysis of 3D-printed implants after 6 months of implantation. Representative μCT images of (A) untreated defect showing empty space (E) and native bone at base of defect (B) and (B) treated defect after 6 months with native surrounding bone (B) and remains of ceramic implant (CI). (C) Quantification of implant volume after printing and after implantation using 3D-reconstructed volumes from μCT images. The arrow indicates the region where new bone was formed. Scale bars are 5 mm. * indicates a significant difference, $p = 0.05$.

specimens with and without implants (Figure 4). Six months after implantation, we observed significantly higher new bone deposition in all of the defects containing 3D-printed implants, compared to the empty defects (Figure 4A,B). Bone ingrowth was found throughout the defect, predominantly inside the implant macropores and in contact with the printed material (indicated by the white arrows in Figure 4B). In contrast, and as expected, the empty defects were not filled with new bone after 6 months. As it was possible to distinguish between the implant geometry and newly formed bone, the implant resorption was quantified by comparing the implants' volume before and after the in vivo period. Approximately 40% of the visible volume of the implants was degraded at 6 months, suggesting that the brushite implants were able to stimulate new bone formation.

Moreover, XRD patterns of implants before and after implantation displayed different CaP phases (Figure 5). Before implantation, the printed implants were predominantly composed of brushite and unreacted TCP phases. After implantation, they were composed of predominantly HA and TCP, suggesting that brushite might have been transformed into less soluble CaP phases by a dissolution−reprecipitation reaction.

3.4. Histological Analysis. Histological analysis on the MMA-embedded sections confirmed the micro-CT findings (Figure 6). Methylene blue and basic fuchsin staining showed new bone ingrowth inside the implants' macropores, together with a tight bond between the newly formed bone and the host bone. In contrast, little new bone formation was detected in the empty defects, which were filled with fibrotic scar tissue.

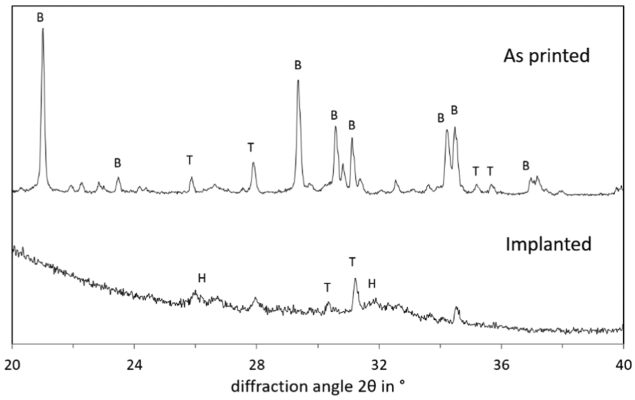

Figure 5. X-ray diffraction analysis of 3D-printed ceramic implants before (as-printed) and after explantation after a 6 month in vivo period. Most prominent peaks of brushite (B), β-tricalcium phosphate (T), and hydroxyapatite (H) are labeled.

Picrosirius red staining confirmed the presence of collagen, and thus mineralized tissue, inside the macropores of the implants and at the implant surface cavities. Only minor traces of mineralized tissue were observed in the empty defects.

4. DISCUSSION

As physical properties and 3D structure of biomaterial constructs are known to be critical to their osteopromoting regenerative performance,[7,26] implant architecture and material characteristics were studied in detail in vitro prior to their in vivo application. The cement system used for 3D printing

https://dx.doi.org/10.1021/acsbiomaterials.9b01819
ACS Biomater. Sci. Eng. 2020, 6, 1681−1689

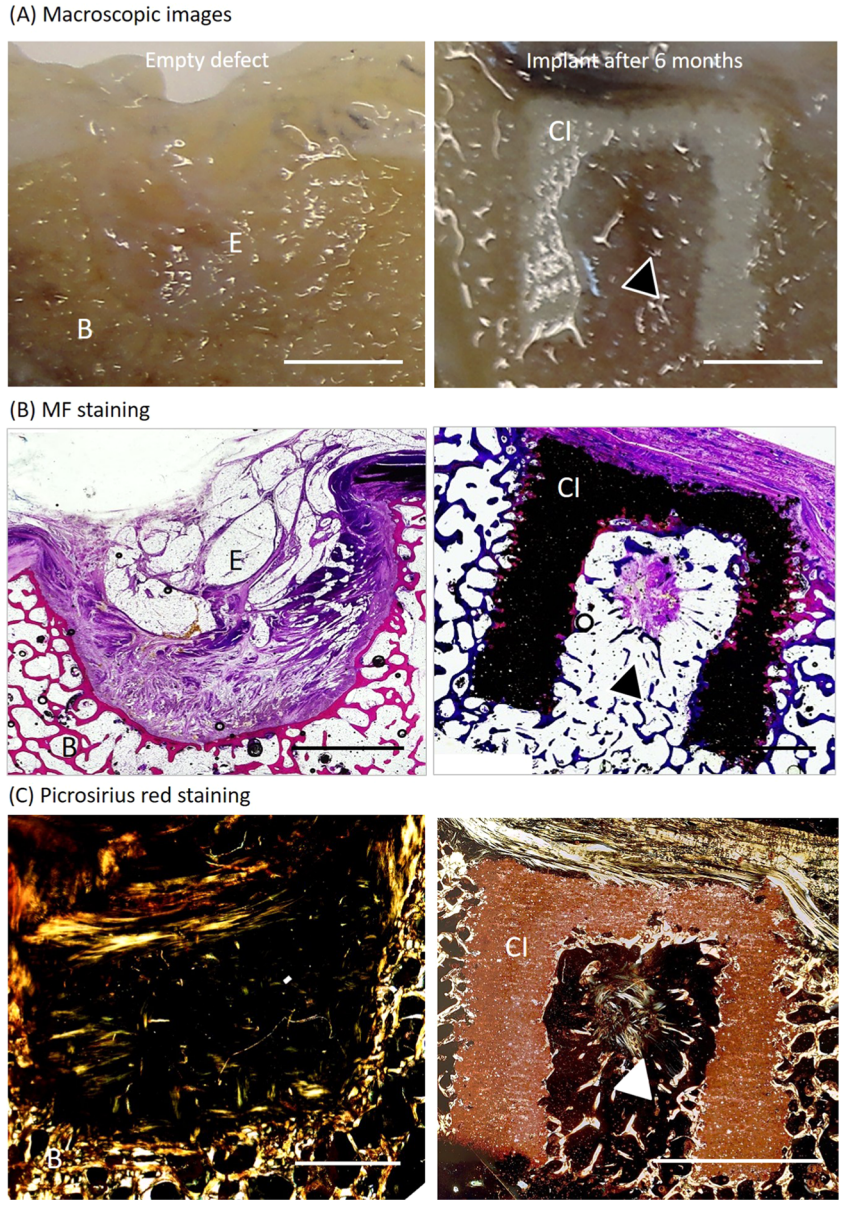

Figure 6. Histologic analysis of 3D-printed implants after 6 months of implantation. Representative images of (A) postmortem processed samples; (B) methylene blue and basic fuchsin (MF)-stained samples; and (C) picrosirius red-stained samples under polarized light. CI—ceramic implant, B—bone, E—empty defect. The arrows indicate some of the regions where new bone was formed. Scale bars are 5 mm.

formed mostly a brushite phase by the reaction of α/β-$Ca_3(PO_4)_2$ (tricalcium phosphate) with a phosphoric acid solution according to

$$\alpha/\beta - Ca_3(PO_4)_2 + H_3PO_4 + 6H_2O \rightarrow 3CaHPO_4{\cdot}2H_2O$$

The high reactivity of the powder−binder system allowed the production of implants with high accuracy and minimal dimensional variations from the computer-designed geometry. These findings confirm the potential of this 3D printing methodology for individual implant fabrication and are in line with our previous results.[10,11,13] Moreover, by using this printing method, we were able to combine a highly soluble ceramic phase with a porous microstructure of around 30%. These two material properties could explain the observed in vivo performance and, in part, explain its osteoconductive and, eventual, osteoinductive properties.

These findings also align well with our previous work, where we demonstrated that brushite-based scaffolds were cytocompatible and improved the osteoblast activity over 7 days in vitro culture.[27] However, longer in vitro studies on brushite and other secondary phosphates are usually hampered by their metastable behavior under culture conditions. We have shown previously that the release of phosphate and the adsorption of calcium and magnesium (including the surface deposition of crystalline reprecipitates) are the main determining factors for the results that are eventually obtained.[28] Such behavior has also been reported for other calcium phosphate phases by others.[29] Further, it has also been shown that deviations in calcium and phosphate concentrations in cell culture medium can drastically influence the differentiation and proliferation behavior of mesenchymal stem cells, leading to cell apoptosis at higher phosphate concentrations.[30] This problem can only be solved by excessive washing and/or preconditioning of the

https://dx.doi.org/10.1021/acsbiomaterials.9b01819
ACS Biomater. Sci. Eng. 2020, 6, 1681−1689

brushite samples, as we have previously shown.[27] However, these interventions, in turn, change the surface/volume composition of the samples. Although it is possible to grow cells on such samples, they will not grow on the original material, but on crystalline reprecipitates composed of HA or whitlockite. The latter phases are, however, detrimental for in vivo dissolution as these phases are two orders of magnitude less soluble than brushite, which may hence lead to a slower in vivo degradation profile. Therefore, we decided to implant unwashed brushite samples to maximize in vivo degradation and also to not perform in vitro osteogenic studies, since the results of such studies would be not directly comparable to the in vivo outcomes for the reasons outlined above.

In addition, it is important to mention that after 6 months of implantation both HA and TCP phases were detected. While the latter is a remaining fraction from the raw powder used for implant printing, HA either stems from newly formed bone mineral or was formed from brushite by a dissolution−precipitation reaction. Although at this time point >35% of the implant volume was resorbed, the formation of HA within the residual implant matrix may slow down the implant's resorption speed due to the low solubility of HA under in vivo conditions. To clarify this point, long-term studies are clearly needed. As an alternative to the CaP-based materials, magnesium phosphates have captured increasing attention since Mg^{2+} ions can suppress the formation of an insoluble HA phase.[31]

The influence of the printing direction on the printed constructs' mechanical properties was carefully characterized. Interestingly, significant improvements were only evidenced under diametral tensile strength for the specimens printed along the z direction. This might be explained by small microporosity differences between the different axes, as we have previously demonstrated.[24,32] Importantly, the final mechanical properties of the implants were in accordance with the strength of the native cancellous bone, 4−12 MPa.[33] Furthermore, the high microporosity obtained was caused by the voids between starting α/β-TCP powder particles and is a relevant characteristic of the 3D powder printing of implants since it has been shown that an implant's microporosity has a strong impact on bone formation by inducing ion exchange and bonelike apatite formation.[24,33] Control over micropore size is possible but not trivial with the powder printing process as it requires alteration of different powder characteristics, for example, particle distribution and powder bed compaction, which will affect the reactivity of the powder−binder system and consequently the hardening mechanism.

It is known that any biomaterial approach aimed at human application needs to undergo not only thorough biocompatibility and toxicity screening but also material characterization in vitro, and ultimately will also need to show proof of in vivo bone regenerative capacity in animal model studies. To the best of our knowledge, no formal consensus has been reached on the ideal animal model to be used for translational studies of biomaterial osteopromotive performance.[34] It has, however, become clear that large animal models are preferable to small laboratory species, as these models are more comparable to humans in terms of intrinsic regenerative capacity.[18] While goats and sheep are the commonly used animal model species for human orthopedic interventions, partly owing to their ease of handling and economic husbandry, bone xenograft compatibility in humans has been shown to be superior for equine bone compared to porcine or ovine bone,[35] and equine bone performed better than human, bovine, or even ovine bone in a sheep subchondral bone model.[36] Importantly, from an animal ethics perspective, neither sheep nor goats themselves constitute target species for bone regeneration studies from a veterinary perspective, while horses perform athletic activities and represent substantial economic and/or emotional value; restoration of osteochondral injury and large bone defects is therefore of great relevance to equine veterinary practice and to equine welfare.

In horses, a bone regeneration and osteoinductivity study has previously been performed in equine third metacarpal bone defects, showing favorable results.[37] However, this defect location is challenging both in terms of surgical approach and in terms of potential for significant discomfort to the horse. There is a long history of osteochondral defect studies for cartilage repair in horses.[38] Prior to any application of a biomaterial as a bone anchor in the biomechanically challenging environment of the equine joint, the proposed biomaterial should show promising bone regenerative potential in an orthotopic location; if it proves unsuccessful here, then it should not be tried in a load-bearing situation, while if promising, further testing in such an application could be warranted. A further advantage of testing bone regeneration in an orthotopic site such as the tuber coxae is the possibility of concurrent investigation of novel therapies at different sites. This was done in the present study with a concurrent study into the effect of osteochondral implants in the stifle joints.[25] This simultaneous study was possible thanks to the very limited (if any) impact of the orthotopic bone implant on the animal. In this way, better use is made of the animals involved in the study, contributing to the refinement and reduction of animal experimentation.[39]

The equine tuber coxae to date have not formally been used as a site for bone regeneration studies, but it has several distinct advantages: It is easily accessible, is representative of long compact bones, and does not affect locomotion of the animals during recovery from anesthesia. In fact, we have refined the technique in ponies and have found that bone defects at this site can be created in the standing sedated animal, using systemic opioids and local anesthetic injections, with the animals showing both great tolerance of the procedure during surgery and an uncomplicated recovery thereafter. The equine tuber coxae bone has also been recently used as a donor site for an equine bone autograft study for mandibular symphysis repair in a horse without significant donor site morbidity or problems with incisional healing.[40] As an anatomical site, the tuber coxae bone is easily accessible, shows little overlying tissue movement during ambulation, and it is remote from the ground, all of which might favor uncomplicated wound healing.

5. CONCLUSIONS

In conclusion, our results provided clinical proof that the 3D-printed brushite implants were able to promote new bone growth after 6 months' implantation in a large animal model, and they degraded by more than one-third in this time. In addition, we demonstrated that the new equine tuber coxae bone model is a promising tool to study the osteopromotive potential of biomaterials in vivo. Further studies, will focus on understanding which cell signaling pathways are activated by the brushite implants, as well as on investigating the effect of implant macropore size and architecture on tissue ingrowth.

https://dx.doi.org/10.1021/acsbiomaterials.9b01819
ACS Biomater. Sci. Eng. 2020, 6, 1681−1689

AUTHOR INFORMATION

Corresponding Author

Miguel Castilho − *Regenerative Medicine Center Utrecht, 3584 CT Utrecht, The Netherlands; Department of Orthopaedics, Division of Surgical Specialties, University Medical Center Utrecht, Utrecht University, 3584 CX Utrecht, The Netherlands;* orcid.org/0000-0002-4269-5889; Email: M.DiasCastilho@umcutrecht.nl

Authors

Rafael Vindas Bolaños − *Cátedra de Cirugía de Especies Mayores, Escuela de Medicina Veterinaria, Universidad Nacional, 86-3000 Heredia, Costa Rica; Department of Equine Sciences, Faculty of Veterinary Medicine, Utrecht University, 3584 CL Utrecht, The Netherlands; Regenerative Medicine Center Utrecht, 3584 CT Utrecht, The Netherlands*

Janny de Grauw − *Department of Equine Sciences, Faculty of Veterinary Medicine, Utrecht University, 3584 CL Utrecht, The Netherlands; Regenerative Medicine Center Utrecht, 3584 CT Utrecht, The Netherlands*

Stefan Cokelaere − *Department of Equine Sciences, Faculty of Veterinary Medicine, Utrecht University, 3584 CL Utrecht, The Netherlands*

Saskia Plomp − *Department of Equine Sciences, Faculty of Veterinary Medicine, Utrecht University, 3584 CL Utrecht, The Netherlands; Regenerative Medicine Center Utrecht, 3584 CT Utrecht, The Netherlands*

Jürgen Groll − *Department of Functional Materials in Medicine and Dentistry, University of Würzburg, D-97070 Würzburg, Germany;* orcid.org/0000-0003-3167-8466

P. René van Weeren − *Department of Equine Sciences, Faculty of Veterinary Medicine, Utrecht University, 3584 CL Utrecht, The Netherlands; Regenerative Medicine Center Utrecht, 3584 CT Utrecht, The Netherlands*

Uwe Gbureck − *Department of Functional Materials in Medicine and Dentistry, University of Würzburg, D-97070 Würzburg, Germany*

Jos Malda − *Department of Equine Sciences, Faculty of Veterinary Medicine and Department of Orthopaedics, Division of Surgical Specialties, University Medical Center Utrecht, Utrecht University, 3584 CL Utrecht, The Netherlands; Regenerative Medicine Center Utrecht, 3584 CT Utrecht, The Netherlands*

Complete contact information is available at: https://pubs.acs.org/10.1021/acsbiomaterials.9b01819

Author Contributions

#R.V.B. and M.C. are shared first authorship.

Notes

The authors declare no competing financial interest.

ACKNOWLEDGMENTS

The research leading to these results has received funding from the Ministerio de Ciencia, Tecnología y Telecomunicaciones de Costa Rica (MICITT), the Consejo Nacional para Investigaciones Científicas y Tecnológicas de Costa Rica (CONICIT), the strategic alliance University Medical Center Utrecht—Technical University Eindhoven, and the Dutch Arthritis Foundation (LLP-12 and LLP-22). In addition, the authors would like to thank Behdad Pouran for technical assistance with μCT analysis and Elke Vorndran for the support with 3D printing and XRD analysis.

REFERENCES

(1) Reichert, J. C.; Cipitria, A.; Epari, D. R.; Saifzadeh, S.; Krishnakanth, P.; Berner, A.; Woodruff, M. A.; Schell, H.; Mehta, M.; Schuetz, M. A.; Duda, G. N.; Hutmacher, D. W. A Tissue Engineering Solution for Segmental Defect Regeneration in Load-Bearing Long Bones. *Sci. Transl. Med.* **2012**, *4*, No. 141ra193.

(2) Olszta, M. J.; Cheng, X.; Jee, S. S.; Kumar, R.; Kim, Y.; Kaufman, M.; Douglas, E.; Gower, L. Bone structure and formation: a new perspective. *Mater. Sci. Eng., R* **2007**, *58*, 77−116.

(3) Urist, M. R. Bone: Formation by autoinduction. *Science* **1965**, *150*, 893−899.

(4) LeGeros, R. Z. Properties of Osteoconductive Biomaterials: Calcium Phosphates. *Clin. Orthop. Relat. Res.* **2002**, *395*, 81−98.

(5) Szpalski, M.; Gunzburg, R. Applications of calcium phosphate-based cancellous bone void fillers in trauma surgery. *Orthopedics* **2002**, *25*, S601−S609.

(6) Rey, C. Calcium Phosphates for Medical Applications. In *Calcium Phosphates in Biological and Industrial Systems*; Amjad, Z., Ed.; Kluwer Academic Publishers: Boston, 1998; pp 217−251.

(7) Yuan, H.; Fernandes, H.; Habibovic, P.; de Boer, J.; Barradas, A. M.; de Ruiter, A.; Walsh, W. R.; van Blitterswijk, C. A.; de Bruijn, J. D. Osteoinductive ceramics as a synthetic alternative to autologous bone grafting. *Proc. Natl. Acad. Sci. U.S.A.* **2010**, *107*, 13614−13619.

(8) Ferraro, J. W. Experimental evaluation of ceramic calcium-phosphate as a substitute for bone grafts. *Plast. Reconstr. Surg.* **1979**, *63*, 634−640.

(9) Cameron, H. U.; MacNeb, I.; Pilliar, R. M. Evaluation of a biodegradable ceramic. *J. Biomed. Mater. Res.* **1977**, *11*, 179−186.

(10) Habibovic, P.; Gbureck, U.; Doillon, C. J.; Bassett, D. C.; van Blitterswijk, C. A.; Barralet, J. E. Osteoconduction and osteoinduction of low-temperature 3D printed bioceramic implants. *Biomaterials* **2008**, *29*, 944−953.

(11) Castilho, M.; Dias, M.; Vorndran, E.; Gbureck, U.; Fernandes, P.; Pires, I.; Gouveia, B.; Armés, H.; Pires, E.; Rodrigues, J. Application of a 3D printed customized implant for canine cruciate ligament treatment by tibial tuberosity advancement. *Biofabrication* **2014**, *6*, No. 025005.

(12) Probst, F. A.; Hutmacher, D. W.; Müller, D. F.; Machens, H. G.; Schantz, J. T. Calvarial reconstruction by customized bioactive implant. *Handchir. Mikrochir. Plast. Chir.* **2010**, *42*, 369−373.

(13) Klammert, U.; Gbureck, U.; Vorndran, E.; Rödiger, J.; Meyer-Marcotty, P.; Kübler, A. C. 3D powder printed calcium phosphate implants for reconstruction of cranial and maxillofacial defects. *J. Craniomaxillofac. Surg.* **2010**, *38*, 565−570.

(14) Gbureck, U.; Hölzel, T.; Klammert, U.; Würzler, K.; Müller, F. A.; Barralet, J. E. Resorbable dicalcium phosphate bone substitutes prepared by 3D powder printing. *Adv. Funct. Mater.* **2007**, *17*, 3940−3945.

(15) Castilho, M.; Moseke, C.; Ewald, A.; Gbureck, U.; Groll, J.; Pires, I.; Teßmar, J.; Vorndran, E. Direct 3D powder printing of biphasic calcium phosphate scaffolds for substitution of complex bone defects. *Biofabrication* **2014**, *6*, No. 015006.

(16) Vorndran, E.; Klarner, M.; Klammert, U.; Grover, L. M.; Patel, S.; Barralet, J. E.; Gbureck, U. 3D Powder Printing of beta-Tricalcium Phosphate Ceramics Using Different Strategies. *Adv. Eng. Mater.* **2008**, *10*, B67−B71.

(17) Tamimi, F.; Corneau, P.; Nihouannen, D.; Zhang, Y.; Bassett, D.; Khalili, S.; Gbureck, U.; Tran, S.; Komarova, S.; Barralet, J. Perfluorodecalin and bone regeneration. *Eur. Cells Mater.* **2013**, *25*, 22−36.

(18) Muschler, G. F.; Raut, V. P.; Patterson, T. E.; Wenke, J. C.; Hollinger, J. O. The Design and Use of Animal Models for Translational Research in Bone Tissue Engineering and Regenerative Medicine. *Tissue Eng., Part B* **2010**, *16*, 123−145.

(19) Frisbie, D. D.; Mc Ilwraith, C. W.; Arthur, R. M.; Blea, J.; Baker, V. A.; Billinghurst, R. C. Serum biomarker levels for musculoskeletal disease in two- and three-year-old racing Thoroughbred horses: A prospective study of 130 horses. *Equine Vet. J.* **2010**, *42*, 643−651.

(20) Gyles, C. One Medicine, One Health, One World. *Can. Vet. J.* **2016**, *57*, 345−346.
(21) Williams, R. B.; Harkins, L. S.; Hammond, C. J.; Wood, J. L. Racehorse injuries, clinical problems and fatalities recorded on British racecourses from flat racing and National Hunt racing during 1996, 1997 and 1998. *Equine Vet. J.* **2001**, *33*, 478−486.
(22) Bigham-Sadegh, A.; Oryan, A. Selection of animal models for pre-clinical strategies in evaluating the fracture healing, bone graft substitutes and bone tissue regeneration and engineering. *Connect. Tissue Res.* **2015**, *56*, 175−194.
(23) Wright, I. M. Racecourse fracture management. Part 1: Incidence and principles. *Equine Vet. Educ.* **2017**, *29*, 391−400.
(24) Castilho, M.; Rodrigues, J.; Pires, I.; Gouveia, B.; Pereira, M.; Moseke, C.; Groll, J.; Ewald, A.; Vorndran, E. Fabrication of individual alginate-TCP scaffolds for bone tissue engineering by means of powder printing. *Biofabrication* **2015**, *7*, No. 015004.
(25) Vindas Bolaños, R. A.; Cokelaere, S. M.; Estrada McDermott, J. M.; Benders, K. E. M.; Gbureck, U.; Plomp, S. G. M.; Weinans, H.; Groll, J.; van Weeren, P. R.; Malda, J. The use of cartilage decellularized matrix scaffold for the repair of osteochondral defects: the importance of long-term studies in large animal model. *Ostearthritis Cartilage* **2017**, *25*, 413−420.
(26) Bose, S.; Roy, M.; Bandyopadhyay, A. Recent advances in bone tissue engineering scaffolds. *Trends Biotechnol.* **2012**, *30*, 546−554.
(27) Schamel, M.; Barralet, J.; Groll, J.; Gbureck, U. *In vitro* ion adsorption and cytocompatibility of dicalcium phosphate ceramics. *Biomater. Res.* **2017**, *21*, No. 10.
(28) Geffers, M.; Barralet, J.; Groll, J.; Gbureck, U. Dual-setting brushite−silica gel cements. *Acta Biomater.* **2015**, *11*, 467−476.
(29) Gustavsson, J.; Ginebra, M. P.; Planell, J.; Engel, E. Osteoblast-like cellular response to dynamic changes in the ionic extracellular environment produced by calcium-deficient hydroxyapatite. *J. Mater. Sci.: Mater. Med.* **2012**, *23*, 2509−2520.
(30) Liu, Y. K.; Lu, Q. Z.; Pei, R.; Ji, H. J.; Zhou, G. S.; Zhao, X. L.; et al. The effect of extracellular calcium and inorganic phosphate on the growth and osteogenic differentiation of mesenchymal stem cells in vitro: implication for bone tissue engineering. *Biomed. Mater.* **2009**, *4*, No. 025004.
(31) Kanter, B.; Vikman, A.; Brückner, T.; Schamel, M.; Gbureck, U.; Ignatius, A. Bone regeneration capacity of magnesium phosphate cements in a large animal model. *Acta Biomater.* **2018**, *69*, 352−361.
(32) Christ, S.; Schnabel, M.; Vorndran, E.; Groll, J.; Gbureck, U. Fiber reinforcement during 3D printing. *Mater. Lett.* **2015**, *139*, 165−168.
(33) Karageorgiou, V.; Kaplan, D. Porosity of 3D biomaterial scaffolds and osteogenesis. *Biomaterials* **2005**, *26*, 5474−5491.
(34) Yang, Z.; Yuan, H.; Tong, W.; Zou, P.; Chen, W.; Zhang, X. Osteogenesis in extraskeletally implanted porous calcium phosphate ceramics: variability among different kinds of animals. *Biomaterials* **1996**, *17*, 2131−2137.
(35) Tetè, S.; Zizzari, V. L.; Vinci, R.; Zara, S.; Di Tore, U.; Manica, M.; Cataldi, A.; Mortellaro, C.; Piattelli, A.; Gherlone, E. Equine and porcine bone substitutes in maxillary sinus augmentation: a histological and immunohistochemical analysis of VEGF expression. *J. Craniofac. Surg.* **2014**, *25*, 835−839.
(36) Waselau, A. C.; Nadler, D.; Müller, J. M.; Zlinszky, K.; Hilbe, M.; Auer, J. A.; von Rechenberg, B. The effect of cartilage and bone density of mushroom-shaped, photooxidized, osteochondral transplants: an experimental study on graft performance in sheep using transplants originating from different species. *BMC Musculoskelet. Disord.* **2005**, *6*, No. 60.
(37) Tsuzuki, N.; Otsuka, K.; Seo, J.; Yamada, K.; Haneda, S.; Furuoka, H.; Tabata, Y.; Sasaki, N. In vivo osteoinductivity of gelatin β-tri-calcium phosphate sponge and bone morphogenetic protein-2 on an equine third metacarpal bone defect. *Res. Vet. Sci.* **2012**, *93*, 1021−1025.
(38) Mcllwraith, C. W.; Frisbie, D. D. Microfracture: Basic Science Studies in the Horse. *Cartilage* **2010**, *1*, 87−95.
(39) Guhad, F. Introduction to the 3Rs (Refinement, Reduction and Replacement). *J. Am. Assoc. Lab. Anim. Sci.* **2005**, *44*, 58−59.
(40) Ogden, N. K. E.; Jukic, C. C.; Zedler, S. T. Management of an extensive equine juvenile ossifying fibroma by rostral mandibulectomy and reconstruction of the mandibular symphysis using String of Pearls plates with cortical and cancellous bone autografts. *Vet. Surg.* **2019**, *48*, 105−111.

https://dx.doi.org/10.1021/acsbiomaterials.9b01819
ACS Biomater. Sci. Eng. 2020, 6, 1681−1689